Snapp: An Agile Robotic Fish With 3-D Maneuverability for Open Water Swim

Timothy J.K. Ng ⬡, Nan Chen ⬡, *Graduate Student Member, IEEE*, and Fu Zhang ⬡, *Member, IEEE*

Abstract—Fish exhibit impressive locomotive performance and agility in complex underwater environments, using their undulating tails and pectoral fins for propulsion and maneuverability. Replicating these abilities in robotic fish is challenging; existing designs focus on either fast swimming or directional control at limited speeds, mainly within a confined environment. To address these limitations, we designed Snapp, an integrated robotic fish capable of swimming in open water with high speeds and full 3-dimensional maneuverability. A novel cyclic-differential method is layered on the mechanism. It integrates propulsion and yaw-steering for fast course corrections. Two independent pectoral fins provide pitch and roll control. We evaluated Snapp in open water environments and demonstrated significant improvements in speed and maneuverability, achieving swimming speeds of 1.5 m/s (1.7 body lengths per second) and performing complex maneuvers, such as a figure-8 and S-shape trajectory. Instantaneous yaw changes of 15° in 0.4 s, a minimum turn radius of 0.85 m, and maximum pitch and roll rates of 3.5 and 1 rd/s, respectively, were recorded. Our results suggest that Snapp's swimming capabilities have excellent practical prospects for open seas and contribute significantly to developing agile robotic fishes.

Index Terms—Bio-inspired robots, biomimetics, robot fish, marine robotics, underactuated control.

I. INTRODUCTION

FISH display exceptional agility in water with their fast swimming and remarkable maneuverability [1]. Tuna fish, for example, have cruising speeds of 1.7 m/s [2] and can make fast turns when catching prey. In addition, there is a growing need for a controllable, field-deployable, fish-inspired robotic platform for underwater applications [3] as they can interact and observe the environment without disturbing its biocenosis [4], [5]. To succeed in open water missions, robot fish designs should mimic fishes in both speed and maneuverability, i.e., agility. This agility depends on their structures and can be categorized into two groups: highly-articulated structure (HAS) and simply-articulated structure (SAS).

The HAS robot fish has a large degree of control over its shape, mimicking waveforms of natural fishes [4], [6], [7], [8].
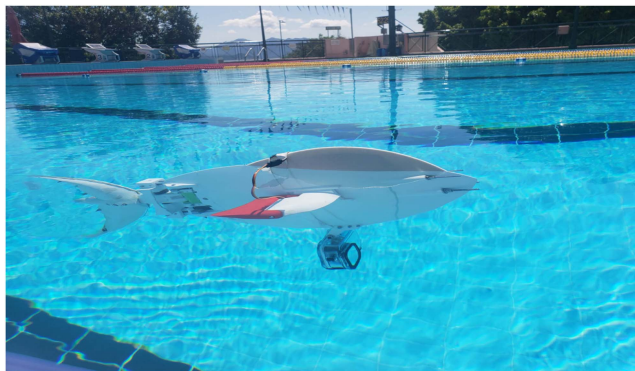
Fig. 1. Snapp, the agile robotic fish deployed in an open water environment with an underwater camera attached to the bottom. It is statically stable in an upright form and can carry payloads of up to 1 kg.
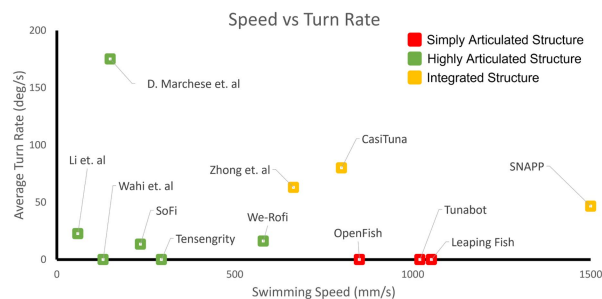

Fig. 2. Distribution of robotic fishes with their swimming speed and average turn rate. The simply (red) and highly (green) articulated structures are at the left and right quadrants; each group focuses on speed or maneuverability, respectively. The integrated approach combines the understanding from both, and result in better performance. [4], [6], [8], [9], [10], [11], [14], [15], [19].

These mechanisms include parallel-series linkages, wire-driven tendon-based skeletons, or soft visco-elastic designs. They have great control over the fish's morphology, with C-shapes yielding fast turns and decent swimming performance with S-shapes. However, they exhibit poor power transmission and a lower actuation frequency ceiling, resulting in lower swimming speeds. In contrast, SAS focus on one actuator driving a scotch-yoke mechanism with high-stiffness fins to recreate fish-like swimming [9], [10], [11]. This mechanism structure effectively replicates the high-frequency tail-beat of Tuna, leading to fast swimming performance. However, this mechanism maneuvers poorly because of its limited control over its morphology. The high-frequency oscillations also cause hydrodynamic recoil, resulting in lateral instability [12], [13]. As the mechanism structure is closely related to its swimming abilities, it is important to integrate both maneuverability and speed in the design process. Fig. 2

summarizes the trade off between speed and maneuverability of these structures.

Recent developments [14], [15], show potential for an agile open water swimmer by integrating speed and maneuverability in their designs. They build upon HAS, improving their performance with swimming speeds and turn rates of about 0.8 m/s and 80 °/s, respectively. Despite this, they report facing problems with lateral stability as they reach higher speeds. [4], [16] highlight the engineering challenges for open water swimming, such as buoyancy, weight, and waterproofing. Integrating these advantages and overcoming their shortcomings for open water swimming is important.

We present Snapp, the first compact robotic fish capable of both fast swims and agile maneuvers in an open water environment. It adopts the SAS and layers a novel-cyclic differential method for yaw control. A bio-inspired flexible caudal fin is attached to the mechanism. These combined improves the maneuverability of the existing SAS with a yaw-turn rate of 46.7 °/s, comparable to the HAS. The pectoral fins leverage the high-swimming speeds for pitch and roll control providing lateral stability and altitude control.

As swimming speed is essential, our mechanism can tune the dimensionless Strouhal number by adjusting the frequency and amplitude parameters on the fly. This allows users to optimize different tail fin parameters during experiments. Snapp is compact and untethered, weighs 5 kg with active and passive stability mechanisms, has a 30-minute continuous operating time, and can carry a payload of up to 1 kg.

Snapp's design is inspired by key carangiform and thunniform swimming features [1], [17], [18]: (i) lunate fin shape, (ii) rapid tail oscillations focused towards the caudal fin [10], and (iii) winged-shaped pectoral fins for stability. Snapp's performance resembles the agility of Tuna with a swimming speed of 1.5 m/s and full 3D maneuverability. It is the first bio-inspired robotic fish to demonstrate advanced swimming capabilities in open water environments by integrating speed, maneuverability, and agility.

II. METHODS, MATERIALS, AND DESIGN

A. Design and Fabrication

The fish chassis and caudal fin are made from Tough Polylactic Acid (TPLA) by 3D printing. These are coated with XTC-4D epoxy resin for waterproofing. The caudal fin has a flexible component made from a 2 mm Polycarbonate sheet. Snapp is powered by a Maxon 150-W, RE40 DC motor (7800 RPM, Maxon GP42 C with a gear ratio of 12:1) and is controlled by a Tritonic ESC 4X motor driver via Pulse Width Modulation (PWM) and is powered by a 24-V LiPo battery. Fig. 3 details the full assembly of Snapp. Two Savox 1211-SG waterproof servos power the pectoral fins. Motor feedback is given by the HEDL 5140 incremental encoder with 500 counts per turn. The Pixhawk microcontroller processes the sensor signal at a sampling rate of 400 Hz. It receives user commands for the throttle, roll, pitch, and yaw and translates them into commands for the pectoral fins and the caudal fin. Underwater communication was achieved using EzUHF 433-MHz, 500-mW Transmitter, and Diversity 8-channel receiver.

B. Bioinspiration and Carangiform Swimming

We take inspiration from the carangiform mode of swimming, with the lateral motion increasing from head to tail. This motion
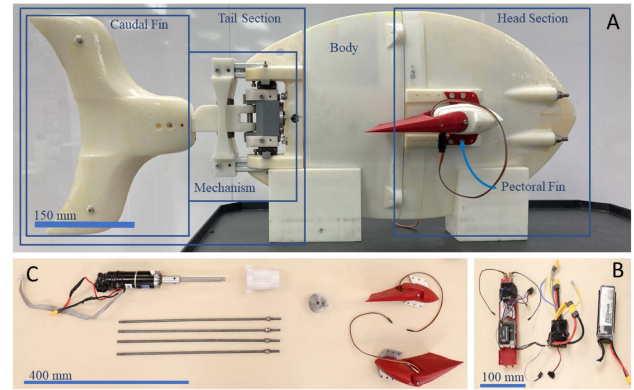

Fig. 3. Detailed components of the robot fish with all components existing inside a compact form factor. (A) The chassis consists of 3 major components, (i) the headpiece, which houses the electronics; (ii) the body, which the motor is mounted to and acts as a support structure; (iii) the tail section, consisting of a scotch-yoke mechanism, pivot lever and a flexible tail. These are combined with stainless-steel tension rods to provide structural rigidity. A modular caudal tail-fin is then attached to the end of the mechanism, with the flexible portion attached directly to the caudal fin. (B) Electricals and electronics of Snapp. (C) The actuators and tension rods. The robot measures a length of 550 mm without the caudal-tail* fin, a width of 74 mm, a height of 292 mm, weighs 5 kg, and is neutrally buoyant and swim for 30 minutes. The caudal fin has a length of 300 mm, with a total length of 850 mm.

$y(x, t)$ closely resembles that of a traveling wave, with x being the normalized length measured from the stationary point on the body [20],

$$y(x, t) = a(x) \sin (kx - \omega_m t), \ a(x) = c_1 x + c_2 x^2 \quad (1)$$

where $k = 2\pi/\lambda$ is the wavenumber and λ, the wavelength the travelling wave, ω, the oscillation frequency associated with the flapping frequency ω_m, and $a(x)$, the amplitude envelope, where c_1 and c_2 are adjustable parameters. We mimic these ratios closely from [10] and realize this with two rigid links consisting of the body (550 mm) and the tail (150 mm), combined with the flexible fin (150 mm).

The lunate-shape fin of real fish [17] inspires the caudal fin design, albeit enlarged compared to natural swimmers. This change increases the volume of water pushed, providing a larger lift surface for improved propulsion. At low frequencies, it acts as a large rudder as the bending is dependent on the frequency. Fig. 5(B) and equation (7) illustrates this effect. Though a large surface would increase drag, the increased bending at high frequencies minimizes this drag area. Since tuna use their pectoral fins to steer and stabilize themselves during high-speed maneuvers, we applied the same principles to the pectoral fins for Snapp.

C. Buoyancy and Passive Vertical Stability

We chose a passive method to maintain stability for design simplicity. Fig. 1 showcases Snapp's static-vertical stability. A heavy bottom ensures that the fish is statically stable. Calibration weights are added until Snapp has slightly positive buoyancy and pitching moments. The large surface areas of the pectoral fins provide drag resistance to rolling moments. This combination ensures a stable system with a stable equilibrium at the vertical.

D. Tail Mechanism Design

We designed a lightweight single motor-actuated mechanism with high tail beat frequencies to achieve high-speed
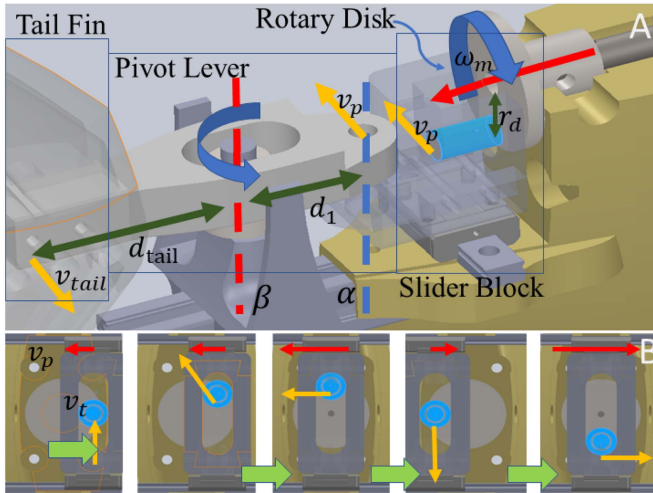
Fig. 4. Tail mechanism in detail. (A) The disk rotates in a circular motion and is connected to the slider-block slot via an extended shaft highlighted in blue. At every rotation point, the shaft on the disk is in contact with the slider block, which is constrained to move in the lateral direction via the linear rail bearings. As the motor rotates with motor speed, ω_m, the slider moves laterally with velocity, v_p. The pivot lever is mounted via a shaft to the slider block at α, which undergoes lateral translation and rotation. The β axis is fixed to the body. The pivot lever rotates about the β axis and can slide freely, i.e., along d_1 causing the distance between axis α and β changes in one tail beat. This results in the end velocity of the tail, v_{tail}. Combined, these act as a see-saw-like lever with β as the fixed rotation axis and V_{tail} as the output. (B) Scotch-yoke in action: Rotational to lateral motion with the tangential velocity, V_p.
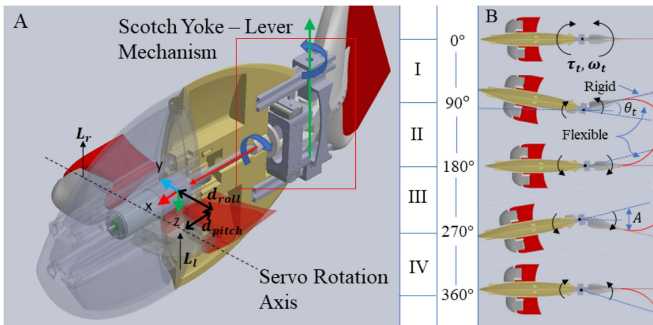

Fig. 5. Actuation of the fish. (A) The pectoral fins are responsible for the dive (i.e., pitch) and roll motions and rotate about the y-axis (blue). The asymmetric angles of the fins create a roll, and similar angles create pitching moments. The motor is positioned in Snapp's head and transmits forces to the mechanism. (B) Mechanism motion and its corresponding tail motion: Phase I starts at 0° to 90° of the rotary disk and rotates counter-clockwise (+). The tail-fin swings right (II, 90° to 180°), back to neutral (III), swings left (IV), and back to neutral. The tail flexes to create an S-shape for fast swimming.

swimming. [21] reports that speed is proportional to frequency for large caudal fins. The tail mechanism is divided into three sections, the scotch-yoke mechanism, a sliding pivot lever, and a flexible caudal fin. Fig. 4 depicts the details of the tail mechanism.

A key parameter in the swimming speed of an undulatory fish is its Strouhal number (St) which is

$$St = fAU^{-1} \tag{2}$$

where f is the tail-beat frequency governed by the motor speed, ω_m, A is the peak-to-peak tail amplitude, and U is the free flow swimming velocity. Fast swimming fish optimize swim at a St

number between 0.3 to 0.4 [22]. We identify an optimal pair of f and A through iterative experiments. We found the highest speed was achieved with a frequency of 4 Hz and a St number of 0.3.

The amplitude parameters, A and θ_t seen in Fig. 5(B) can be adjusted by changing d_1 (Fig. 4) with the following:

$$A = d_{\text{tail}}r_d d_1^{-1}, \; \theta_t = \arctan\left(r_d d_1^{-1}\right) \tag{3}$$

where d_{tail} is the tail length from the β axis, r_d the rotary disk radius, and d_1 the distance between β and α axis. The maximum tail angle of attack is 30°. The flexibility of this design allows us to tune St accordingly.

The lateral undulation of the swimming fish is realized with the scotch yoke mechanism. Fig. 4(A) depicts the kinematics of the mechanism. With a fixed motor speed, the slider block moves with a sinusoidal lateral velocity, v_p, which acts on the pivot lever. The relations are given as

$$v_{\text{tail}} = v_p d_{\text{tail}} d_1^{-1}, \; v_p = r_d \omega_m \cos\theta_m \tag{4}$$

where θ_m is the angle of the rotary disk, and ω_m, the motor speed. Solving for v_{tail} yields

$$v_{\text{tail}} = K\omega_m \cos\theta_m, \; K = r_d d_{\text{tail}} d_1^{-1} \tag{5}$$

with the mechanical constant, K.

Another factor for fast swimming is the S-like bends of a fish as described in Fig. 5(B). We replicated this with a compliant tail of a suitable stiffness. The deflection of the flexible portion of the caudal fin depends on the caudal fin's acceleration, a_{tail}. We can find a_{tail} by differentiating v_{tail} (5) with respect to time to yield

$$a_{\text{tail}} = K\left(\dot{\omega}_m \cos\theta_m + \omega_m^2 \sin\theta_m\right) \tag{6}$$

We assume a steady-state operation during swimming. Then $\dot{\omega}_m = 0$ to give a_{tail}

$$a_{\text{tail}} = K\omega_m^2 \sin\theta_m \tag{7}$$

A higher tail acceleration leads to larger deflections of the flexible fin, which results in an increased thrust force due to the favorable angle of attack. These features combined make Snapp an agile swimming fish.

III. ACTUATION AND CONTROL

The hydrodynamics of fish swimming is complex as it involves elements of vorticity and non-linear fluid dynamics. We proposed a set of control actions with outputs that are strictly increasing to stabilize and control Snapp. Fig. 5(A) shows the actuation mechanisms of Snapp, where the pectoral fins control roll and pitch, and the caudal fin controls yaw. We have an element-normalized control input vector

$$u = [u_a \; u_s \; u_r \; u_p]^T \tag{8}$$

where u_a, u_s, u_r, and u_p are the normalized motor average voltage, the normalized amplitude of the square-wave voltage for yaw control, and the normalized control inputs for roll and pitch, respectively.

A. Actuation of Pitch, Roll, and Altitude

The pectoral fins act as the control surface for pitch and roll by inducing torques about their respective axis. They are speed dependent, and are governed by the lift principle,

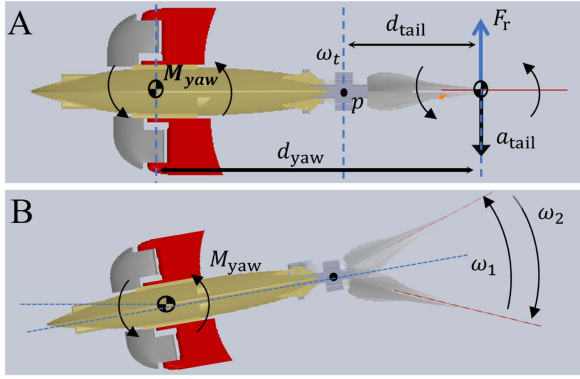$$L(\theta, V) = \frac{1}{2}\rho_w c_L(\theta)SV^2 \tag{9}$$

Fig. 6. Yaw forces on the fish. (A) Active torque applied by the caudal fin on the water. (B) Left turn from a net clockwise M_{yaw} with $\omega_2 > \omega_1$.
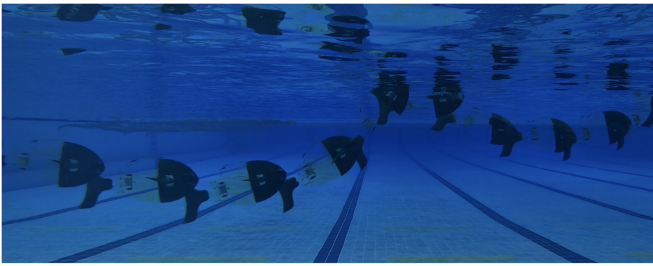

Fig. 7. Overlay of the dive experiment from the stationary underwater camera. The image captures the dive and lift sequence of the robot fish. At the 24.5 s mark, a positive pitch command (dive) of 0.5 was issued. Snapp descended with a maximum pitch angle of $-10°$ and then leveled back to $0°$.
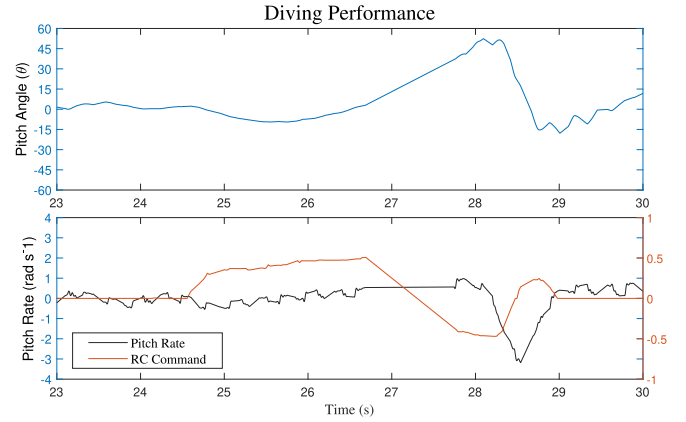

Fig. 8. Plot of the angular position and angular rate with respect to time given the user commands. The pitch is set in an inverted Y mode. When the pitch stick is lowered (-) the pectoral fins are lowered, creating an upward lift, increasing the pitch angle, and providing vertical lift. Angular pitch rate (bottom) responds timely to the dive command and the resurface command. The RC commands are configured in an inverse Y.

where the hydrodynamic parameters c_L, V, S, ρ_{w} as the lift coefficient, swimming velocity relative to the water, control surface fin area, and water density, respectively. θ is the angle of attack of the respective control surfaces, controlled by the user, and is related to the control input by

$$\begin{bmatrix} \theta_l \\ \theta_r \end{bmatrix} = K \begin{bmatrix} 1 & 1 \\ 1 & -1 \end{bmatrix} \begin{bmatrix} u_r \\ u_p \end{bmatrix} \tag{10}$$

where θ_l and θ_r are the angle of attack of the left and right pectoral fins, and K is the constant mapping coefficient. Fig. 5(A) shows the corresponding forces and their moment arms. The fish lift (F_z), the roll (M_{roll}), and pitch (M_{pitch}) moments, are calculated by

$$\begin{bmatrix} F_z \\ M_{\text{roll}} \\ M_{\text{pitch}} \end{bmatrix} = \begin{bmatrix} 1 & 1 \\ d_{\text{roll}} & d_{\text{roll}} \\ d_{\text{pitch}} & d_{\text{pitch}} \end{bmatrix} \begin{bmatrix} L(\theta_l, V) \\ L(\theta_r, V) \end{bmatrix} \tag{11}$$

with d_{pitch} and d_{roll} as the respective moment arms. The control authority of the pitch, roll, and altitude is guaranteed with sufficiently large forward swimming speed. Snapp's fast-swimming speed ensures this control authority with faster dive rates. In comparison to other robot fish [4], [14], Snapp does not need an added ballast tank (pressure sensitive) for control over F_z, M_{roll} and M_{pitch}, hence reducing system complexity. This also allows Snapp to swim at any depths.

B. Actuation of Yaw

The yaw actuation of Snapp is an underactuated mechanism as the forward thrust and the yaw-turn moment are accomplished

by the single caudal fin. Ng et al. [23] attempted to course correct the lateral swimming drift on their scotch-yoke mechanism using a speed differential while [19] demonstrated the key to fast turns is a rapid first stroke in a C shape (phase II-III) followed by a slower return stroke (phase IV-I). We built on these ideas and proposed a cyclic differential algorithm that can have fast turns while maintaining swimming speed. We did this by modulating the motor voltage,

$$u_t = (u_a + u_s \text{sign}(\sin(\theta + \phi + \gamma_0))) V_t \tag{12}$$

where u_t is the total voltage applied on the motor; u_a is the average voltage to produce thrust and is proportional to the steady-state motor speed ω_{m}; u_s is the differential amplitude of the square-wave voltage controlled by the user; θ_{m} is the angular position of motor measured by an encoder which indicates the position of caudal-fin; ϕ is the initial phase of the sin function; γ_0 is a constant angle to compensate the response delay and can be calibrated; and V_t the terminal voltage. The square-wave voltage is then generated by applying a sign function on a sine function.

This results in a fin stroke with different speeds. To achieve a left turn (depicted in Fig. 6(B)), the first stroke is slower with the tail angular speed, ω_1, and the return stroke with a faster tail angular speed, ω_2, and vice versa for the right turn. Fig. 6 shows the respective motions and their forces.

To find M_{yaw}, we need to find the water reaction forces, F_{r}, acting with a moment arm, d_{yaw}, on the tail fin. With the added mass principle [18], we get the following

$$F_r = m_w a_{\text{tail}}$$

$$M_{\text{yaw}} = d_{\text{yaw}} F_r \tag{13}$$

where m_{w}, the virtual mass accelerated with the same acceleration as the tail, a_{tail}, which is proportional to ω_{m}^2 (7). The yaw moment per tail beat, M_{cycle}, is derived by taking the difference over the phases as in Fig. 5, with (phase II-III) and right stroke (phase IV-1) as implemented by (12), with the corresponding angular speeds ω_1 and ω_2 respectively. We finally derive M_{cycle} as a function of u_{s}

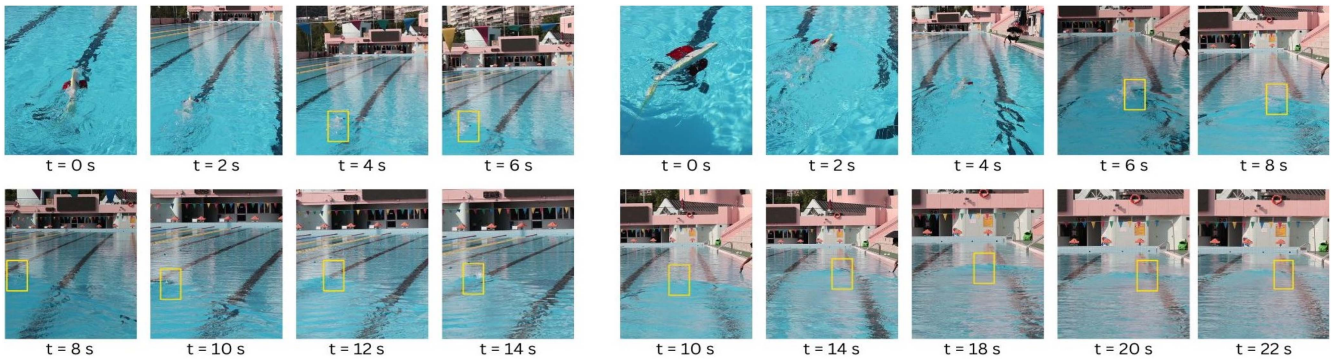$$M_{\text{cycle}} = M(\omega_1) - M(\omega_2) = M(u_s) \tag{14}$$

Fig. 9. (Left) Snapp swimming a 25 m distance without any compensation. The robot fish drifts off to the left side. (Right) Snapp swimming 25 m with roll compensation. Snapp is capable of swimming within the boundary of the 2.5 m lanes.
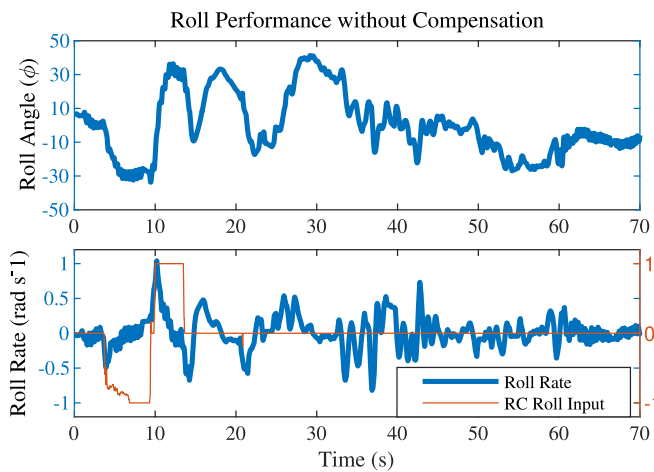

Fig. 10. Step response and natural drift: An initial short impulse was applied to test the response of the system. The roll changes are immediate and responsive. Without any active input, there is a large natural drift to the left caused by the roll instability.
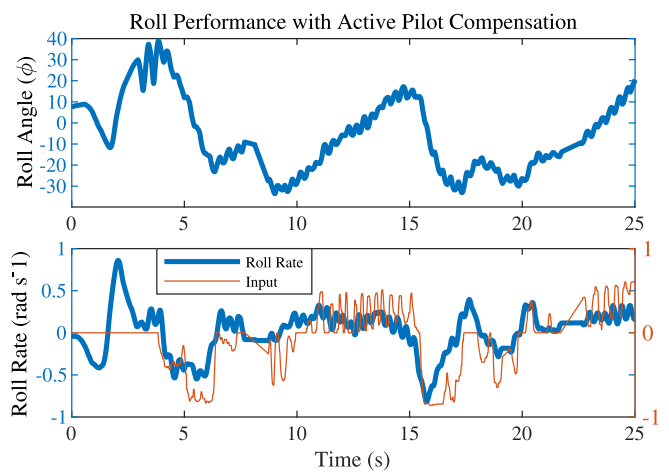
Fig. 11. Active roll compensation controlled by the pilot. By controlling the roll, the pilot is capable of controlling the yaw. A positive roll induces a positive yaw. Data showcases the commands throughout the swim, their corresponding roll angle, and roll rates.

By modulating the difference in motor speed between tail beat cycles, we can control the overall turn rate per stroke. In the absence of the differential, the swimming gait is symmetric, i.e. the lateral swings of the phases are equal in magnitude and cancel out.

IV. RESULTS AND ANALYSIS

To achieve 3D maneuverability, responsive attitude control is required. To demonstrate this, we conducted experiments for each specific attitude, pitch, roll, and yaw. The angular positions and velocities are sampled at 400 Hz, and video recordings above and underwater were taken to track the trajectory of the robot. The results highlight Snapp's system response and its trajectory.

Snapp was tested at two tail actuation at two modes, 2.7 Hz and 4 Hz, determined by measuring the time to complete a 25 m swim course. The average swimming speed associated with the 2.7 Hz and 4 Hz were 1 m/s and 1.5 m/s respectively, demonstrating a 50% increase in swimming speed. For each attitude, we tested the control inputs (8) with pitch, roll and yaw governed by u_p, u_r, u_s respectively, with the swimming speed kept constant. The roll and pitch tests were conducted at a 1 m/s speed. This establishes the minimum speed required for effective control. Finally, we swam Snap in a figure-8 pattern with an initial steady-state pitch angle of 60° to test the robustness of the control methods to disturbances.

A. Field Experiments and Protocols

The experiments were carried out in a swimming pool of 25 m × 25 m with an average depth of 1.2 m. Two cameras captured the video footage of the swimming fish. The first camera was positioned at the starting point of the test, and the second underwater camera was positioned parallel to the swimming direction. A drone camera captured overhead footage for a figure-8 swim. The pilot controls the fish in all experiments.

B. Pitch and Dive Control

The emphasis of this experiment is to control the dive and ascend actions of Snapp. The pectoral fins exert a lift force and a moment as mentioned in Section III(A). These forces contribute to the vertical translation and pitch rotation. To showcase this, Snapp performed the U-shape trajectories in Fig. 7. Snapp initially swam without commands, followed by a dive, then an ascend command. Fig. 8 highlights the relationship between

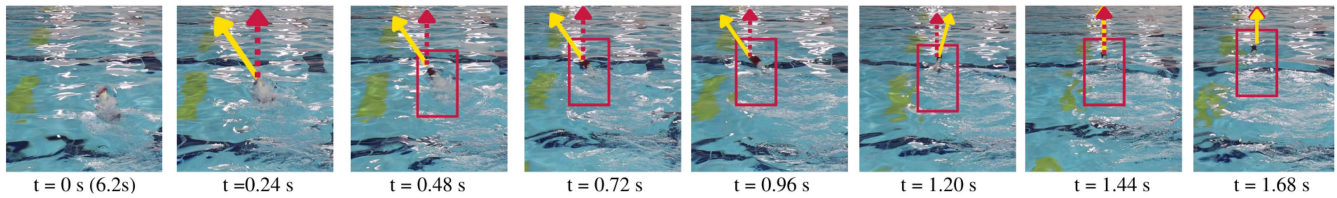| t = 0 s (6.2s) | t =0.24 s | t = 0.48 s | t = 0.72 s | t = 0.96 s | t = 1.20 s | t = 1.44 s | t = 1.68 s |

Fig. 12. Snapp performing a sharp yaw correction. Snapp was initially headed north-west (yellow line) with the red line (dotted) as reference north. Within a single tail-beat (0.96–1.44 s), it corrects its heading to complete the full 25 m swim. Note that the left yellow marker of the swimming pool is the same in all pictures.

the pitch command, and its angle and rate. This dive action corresponded to a maximum positive pitch rate of 0.5 rd/s as seen in the rate plot of Fig. 8. Snapp then ascended with a maximum rate of -3 rd/s (average of 1.5 rd/s) following the ascend command. Finally, at the 28.5 s mark, there was a rapid increase in pitch rate following the ascending stage. This rapid increase is resulted from Snapp leaping out of the water and later falling due to gravity.

Despite the commands between dive and ascend having the same magnitudes (0.5), they have different pitch rates. There are two major reasons for this: (i) an initial offset pitch and (ii) a pitching moment from the caudal fin. Both factors contributed to a positive pitch of Snapp. The former was caused due to water seeping into the shell, thus having a moment imbalance, and the latter is caused by the thrust vector acting below the center of mass, inducing an upward pitch moment. Nevertheless, the pilot completed the U-shape trajectory despite the disturbances.

C. Roll Control and Straight Line Swimming

The roll test was conducted by measuring the roll angles and rates over a 25 m swim course. It is observed that a change in roll causes Snapp to deviate from a straight line. This is because Snapp has a net pitching moment from the caudal fin as the thrust force vector acts below the center of mass. The combined pitching and rolling moments induced a lateral drift. Fig. 9(left) highlights the natural lateral drift that occurs without compensation.

To test the pectoral fin's ability to control roll, we tested (i) a step response, (ii) a straight swim without compensation, and (iii) a straight swim with roll compensation. The roll angle and rate are measured with the user commands. The commands control the roll moments, which reach equilibrium due to the buoyancy moment.

The step response of the roll command was observed in Fig. 10. The results showed a 35° angle in their respective directions in 2 s. The first step input has a maximum roll rate of -0.5 rd/s, and the second has a maximum roll rate of 1 rd/s. Snapp then swam without compensation. The roll drifted and eventually swam out of bounds of the test site with a lateral drift of 5 m from the starting point. In contrast, Fig. 11 shows the step response when active roll compensation is applied by the pilot, highlighting the pilot's attempt to stabilize the roll angle. The roll compensation has a response time of 0.5 seconds and a maximum angular rate of 0.6 rd/s at a swimming speed of 1 m/s. Note that the roll rates followed the commands closely as the pilot adopted a bang-bang (10–15 s) control method. As a result, Snapp swam within the 2.5 m bounds of a standard swimming lane.
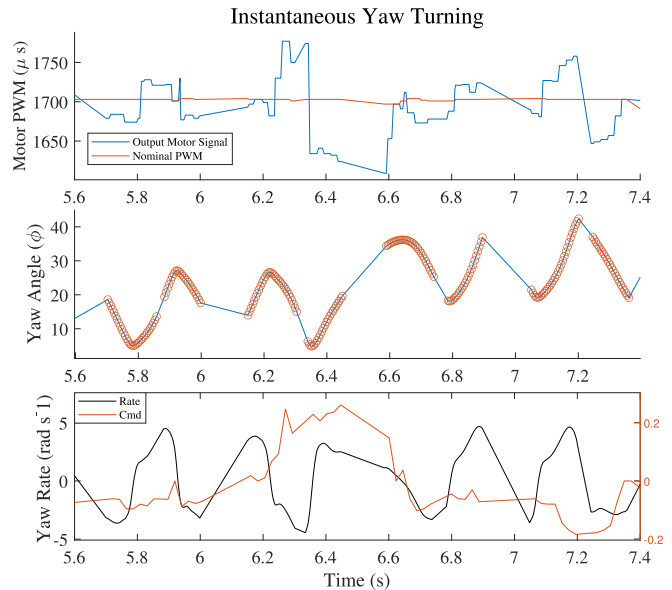

Fig. 13. Sharp yaw correction. (Top) Differential algorithm in action represented by motor output. (Middle) The yaw angle of the swimming fish. (Bottom) The corresponding yaw rates to the instantaneous correction. The command was executed at the 6.2 s–6.6 s mark.

D. Yaw Control for Straight Line Swim

We tested the cyclic-differential method (12) for instantaneous and cruising turns. The pilot was instructed to swim northwest, perform a sharp correction towards the north, and swim to the endpoint at max speed.

Figs. 12 and 13 highlights a sharp yaw turn executed within one tail beat. This command was executed at the 6.2–6.6 s of the swim with a peak-to-peak motor speed differential of 6.24 rd/s (25% of maximum motor speed at 4 Hz). Note that the maximum differential corresponded with a peak-to-peak voltage difference of 20 V or an 80% speed difference. This command, u_s, with value 0.2, changed the angle from an 15° (avg) to a 28°(avg) in 0.4 s, with an yaw rate(avg) of 40°/s. Coinciding with the commands, the angular rate in Fig. 13 (bottom) had a short negative section (6.2 s–6.4 s), followed by a much longer positive yaw rate (6.4 s–6.6 s) before returning to the original swimming pattern. Fig. 14 shows the full timeline of the straight swim. Snapp responded to a left turn command (-0.08) at the (2–6 s) mark. The yaw angle changed from 40° to 15° in that period, with a yaw rate (avg) of 6.25 °/s. The latter part showed the pilot's adjustments to complete the straight swim with 25° as the target. This shows
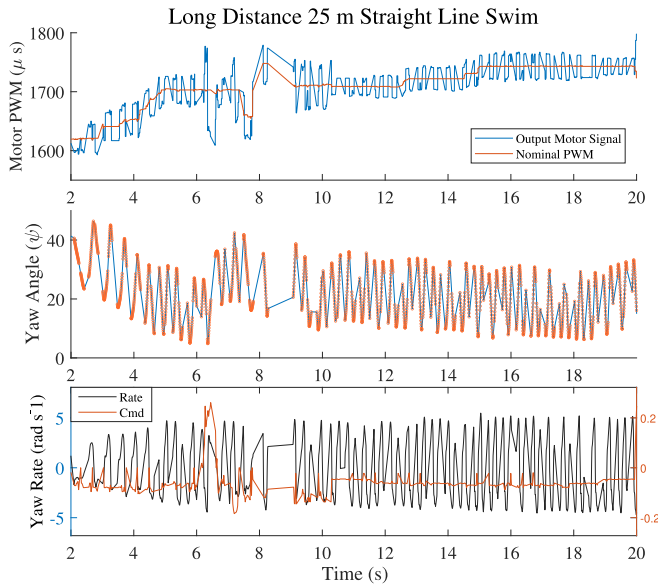
Fig. 14. Full experiment over 25 m. (Top) Motor signals and the modulated signals from the cyclic-differential method. (Middle) Yaw angles of the entire swim. (Bottom) Yaw rates and their corresponding commands.
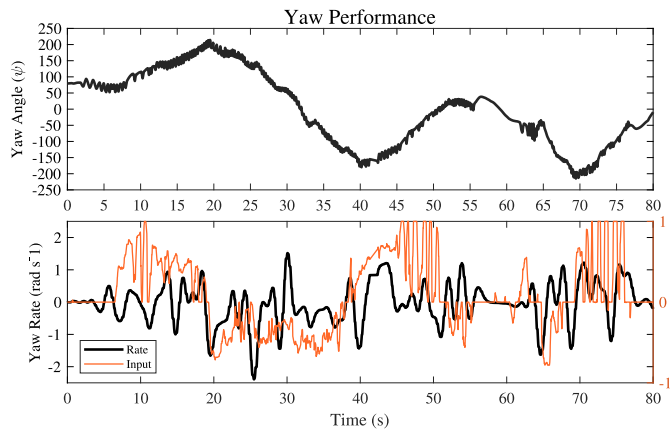

Fig. 15. Figure-8 and S curve data set. (Top) The yaw angle and the pilot's input. (Bottom) The yaw rate closely follows the command by the pilot. The yaw rate was averaged over two tail beats. The 20 s corresponds to the first half of the circle, and the next 20 s corresponds to a full circle, from $200°$ to $-180°$. The 60–80 s corresponds to the S-curve as the fish returned to the starting point. The 20 s mark is the first turning point of the figure-8. The figure-8 and S-curve were completed in one take.

the effectiveness of our cyclic-differential method in controlling yaw.

E. Open Water Swimming: Figure-8 and S Curve.

Snapp completed a figure-8 trajectory followed by an S-curve using all control commands simultaneously. A person piloted the experiment. The commands with their respective angles and velocities were recorded and plotted in Fig. 15. Fig. 16(A) and Fig. 17 depicts the figure-8 attempt and the S-curve, respectively.

Initially, Snapp was held by a person and then released when the tail begins to move. Its natural state was to sink and to have a $90°$ pitch angle as in Fig. 16(C). This state approximates the
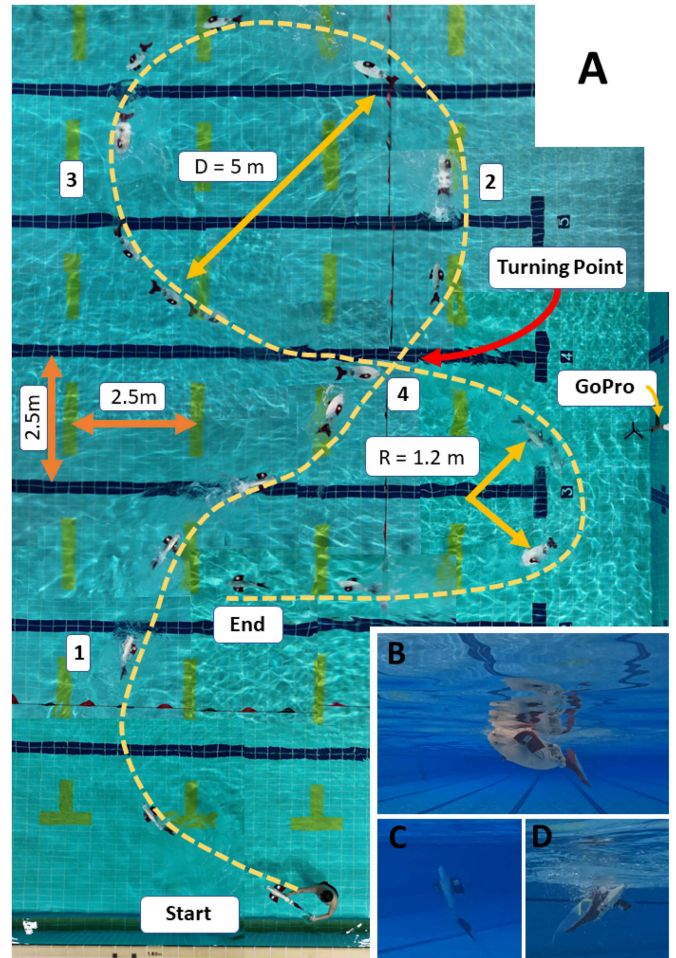

Fig. 16. (A) Aerial view of the figure-8 experiment. The fish swims from the start point, follows the order 1-2-3-4, and finally to the endpoint. The image was generated by manually piecing together different snapshots of the video captured by an aerial drone. (B) Snapp making a turn using a combined roll and yaw. (C) Snapp's neutral state with negative buoyancy and a $90°$ pitch angle. (D) Snapp exits circle 4 and accelerates out. The caudal fin is flexed for maximum propulsion.

uncertainty of open sea swimming, where the initial balance of the fish could be disrupted. Despite the disturbances, the pilot completes the figure-8 and S-curve trajectory. Fig. 15 shows the data collected in this maneuver.

At this point, the turn rate changed from 1 rd/s to -1.5 rd/s, following the command closely. Similar trends occurred throughout the swim, with the 40 s mark representing the second turning point. The average yaw is calculated from the gradient of the yaw-angle graph. At the 60 s mark, the pilot initiates a burst swim followed by a turn maneuver (65 s) and results in a sharp turn of $95°$ in 2 s, a turn rate of 46.7 $°$/s (0.81 rd/s). The top and bottom loop in Fig. 16 has a turning radius of 5 m, and 2.4 m, respectively. The minimum turn radius of 0.83 m (1 BL/s) is observed in the S-curve. Fig. 16(B, C, D) shows the different pitches and rolls during this swim.

Finally, we successfully swam Snapp in the open sea of Hong Kong's Repulse Bay beach. These experiments are available in the video link.

Fig. 17. Aerial view of the S-curve experiment. Snapp swims from the end of figure-8 and completes the S-curve to return to the starting point of the experiment.

V. DISCUSSIONS AND FUTURE WORK

Snapp's swimming efficiency, evaluated by its cost of transport (COT) [24] ranges from 20–35 J/kg/m. Snapp's efficiency is comparable to the lowest COT's [10], [15], with a COT of 27.8 J/kg/m (at 1 m/s, 14.8 Hz) and 17 J/kg/m (at 0.67 m/s, 3 Hz), respectively, suggesting a new motion archetype that is agile yet efficient. Future studies will investigate the effect of mechanism design, swimming gait, and tail-fin design on its efficiency.

Biomimetics is crucial to creating environmental-friendly technology [25]. SoFi explored this and showed that it can swim next to wildlife without scaring them. [26] has shown that robot interaction with flies can increase their mating productivity. Future work can study the interactions between Snapp and wildlife, with the potential for ecological growth and repair.

Snapp's remarkable advancements in speed and maneuverability pushed the boundaries of robotic fish performance in open-water environments. It can be used to observe coral reefs and aquatic life, assist in aquaculture, perform underwater search-and-rescue missions, monitor water quality, assist in marine infrastructure maintenance, and perform stealthy surveillance in maritime security. Snapp is particularly suitable for coastal applications as it has the power to swim against rough wave currents [27] and its compact form allows it to maneuver through complex topography and channels where ROVs and passenger boats have difficulty traversing.

REFERENCES

[1] G. V. Lauder, E. J. Anderson, J. Tangorra, and P. G. A. Madden, "Fish biorobotics: Kinematics and hydrodynamics of self-propulsion," *J. Exp. Biol.*, vol. 210, no. 16, pp. 2767–2780, 2007.

[2] B. A. Block, D. Booth, and F. G. Carey, "Direct measurement of swimming speeds and depth of blue marlin," *J. Exp. Biol.*, vol. 166, no. 1, pp. 267–284, 1992.

[3] T. Castro-Santos, E. Goerig, P. He, and G. V. Lauder, "Applied aspects of locomotion and biomechanics," *Fish Physiol.*, vol. 39, pp. 91–140, 2022.

[4] R. K. Katzschmann, J. DelPreto, R. MacCurdy, and D. Rus, "Exploration of underwater life with an acoustically controlled soft robotic fish," *Sci. Robot.*, vol. 3, no. 16, 2018, Art. no. eaar3449.

[5] S. K. Rajendran and F. Zhang, "Design, modeling, and visual learning-based control of soft robotic fish driven by super-coiled polymers," *Front. Robot. AI*, vol. 8, 2022, Art. no. 809427.

[6] X. Liao, C. Zhou, Q. Zou, J. Wang, and B. Lu, "Dynamic modeling and performance analysis for a wire-driven elastic robotic fish," *IEEE Robot. Automat. Lett.*, vol. 7, no. 4, pp. 11174–11181, Oct. 2022.

[7] B. Chen and H. Jiang, "Swimming performance of a tensegrity robotic fish," *Soft Robot.*, vol. 6, no. 4, pp. 520–531, 2019.

[8] Z. Li, L. Ge, W. Xu, and Y. Du, "Turning characteristics of biomimetic robotic fish driven by two degrees of freedom of pectoral fins and flexible body/caudal fin," *Int. J. Adv. Robot. Syst.*, vol. 15, no. 1, 2018, Art. no. 1729881417749950.

[9] D. Chen, Z. Wu, Y. Meng, M. Tan, and J. Yu, "Development of a high-speed swimming robot with the capability of fish-like leaping," *IEEE/ASME Trans. Mechatron.*, vol. 27, no. 5, pp. 3579–3589, Oct. 2022.

[10] J. Zhu, C. White, D. K. Wainwright, V. D. Santo, G. V. Lauder, and H. Bart-Smith, "Tuna robotics: A high-frequency experimental platform exploring the performance space of swimming fishes," *Sci. Robot.*, vol. 4, no. 34, 2019, Art. no. eaax4615.

[11] S. C. Van Den Berg, R. B. Scharff, Z. Rusák, and J. Wu, "Openfish: Biomimetic design of a soft robotic fish for high speed locomotion," *HardwareX*, vol. 12, 2022, Art. no. e00320.

[12] P. W. Webb, "Is the high cost of body/caudal fin undulatory swimming due to increased friction drag or inertial recoil," *J. Exp. Biol.*, vol. 162, no. 1, pp. 157–166, 1992.

[13] P. W. Webb and D. Weihs, "Stability versus maneuvering: Challenges for stability during swimming by fishes," *Integrative Comp. Biol.*, vol. 55, no. 4, pp. 753–764, 2015.

[14] S. Du, Z. Wu, J. Wang, S. Qi, and J. Yu, "Design and control of a two-motor-actuated tuna-inspired robot system," *IEEE Trans. Syst. Man Cybern.*, vol. 51, no. 8, pp. 4670–4680, Aug. 2021.

[15] Y. Zhong, Z. Li, and R. Du, "A novel robot fish with wire-driven active body and compliant tail," *IEEE/ASME Trans. Mechatron.*, vol. 22, no. 4, pp. 1633–1643, Aug. 2017.

[16] D. Romano, A. Wahi, M. Miraglia, and C. Stefanini, "Development of a novel underactuated robotic fish with magnetic transmission system," *Machines*, vol. 10, no. 9, 2022, Art. no. 755.

[17] M. J. Lighthill, "Aquatic animal propulsion of high hydromechanical efficiency," *J. Fluid Mech.*, vol. 44, no. 2, pp. 265–301, 1970.

[18] L. M. J., "Hydromechanics of aquatic animal propulsion," *Annu. Rev. Fluid Mech.*, vol. 1, no. 1, pp. 413–446, 1969.

[19] A. D. Marchese, C. D. Onal, and D. Rus, "Autonomous soft robotic fish capable of escape maneuvers using fluidic elastomer actuators," *Soft Robot.*, vol. 1, no. 1, pp. 75–87, 2014.

[20] D. S. Barett, M. S. Triantafyllou, M. S. Yue, D. K. P. Grosenbaugh, and M. Wolfgang, "Drag reduction in fish-like locomotion," *J. Fluid Mech.*, vol. 392, pp. 183–212, 1999.

[21] S. Gupta, T. J. K. NG, S. Zhong, and Z. Wang, "Development of high performance mechanical robotic fish," in *Proc. Adv. Maritime Eng. Conf.*, Busan, Oct. 9–12, 2018.

[22] G. K. Taylor, R. L. Nudds, and A. L. Thomas, "Flying and swimming animals cruise at a Strouhal number tuned for high power efficiency," *Nature*, vol. 425, pp. 707–711, 2003.

[23] T. J. K. NG, C. C. Tang, and Z. Wang, "Caudal-fin based turning mechanism for an underactuated fast swimming robotic fish," in *Proc. Adv. Maritime Eng. Conf.*, SMTU, St. Petersburg, Russia, 2021.

[24] K. Schmidt-Nielsen, "Locomotion: Energy cost of swimming, flying, and running," *Science*, vol. 177, no. 4045, pp. 222–228, 1972.

[25] F. Meder et al., "A perspective on plant robotics: From bioinspiration to hybrid systems," *Bioinspiration Biomimetics*, vol. 18, no. 11, 2022, Art. no. 015006.

[26] D. Romano, G. Benelli, and C. Stefanini, "How aggressive interactions with biomimetic agents optimize reproductive performances in mass-reared males of the mediterranean fruit fly," *Biol. Cybern.*, vol. 117, pp. 1–10, 2023.

[27] T. Scott, M. Austin, G. Masselink, and P. Russell, "Dynamics of rip currents associated with groynes–field measurements, modelling and implications for beach safety," *Coastal Eng.*, vol. 107, pp. 53–69, 2016.